J Ther Eng, Vol. 11, No. 4, pp. 1023–1038, July, 2025

Journal of Thermal Engineering
Web page info: https://jten.yildiz.edu.tr
DOI: 10.14744/thermal.0000961

Research Article

An in-depth numerical investigation of a solar latent heat storage unit incorporating phase change materials

Kenza OUDAOUI[1], Mustapha FARAJI[1,*]

[1]*Hassan II Univesity, Faculty of Sciences Ain Chock, 20100, Casablanca, Morocco*

ARTICLE INFO

Article history
Received: 18 June 2024
Revised: 26 September 2024
Accepted: 30 September 2024

Keywords:
Heat Discharge; Heat Exchangers; Heat Transfer; Latent Heat Storage; Phase Change Materials; Solidification Process; Solar Energy; Water Heating

ABSTRACT

The energy storage method is very important for many engineering domains, providing multiple benefits for a variety of fields. The requirement for an effective way to store heat generated during times of high solar radiation and, recover it later when there is no sun is one of the most frequent issues that solar power systems encounter. Therefore, storing energy using phase change materials (PCM) is an important solution for overcoming the mismatch between the energy supply and demand in solar thermal systems. We study a new heat storage system based on 3 different phase change materials and not on a single one. Most of the previous studies focus on charging or storing heat in a PCM. But crucial problems arise during discharge. Given the low thermal conductivity of the phase change materials, are we able to recover all the energy we have stored and how? This is the major objective of this study. The novel heat storage unit uses three different phase change materials instead of one. These phase change materials are located at variable positions to optimize the performance of the latent heat storage unit. The main purpose of the present paper is to numerically study the discharge process of multiple phase change materials in a coaxial solar water/PCM heat exchanger. Different configurations, including the phase change material position and PCM thickness are analyzed. These materials were selected according to their thermophysical properties (melting temperature, thermal conductivity and latent heat of fusion). For this purpose, a cylindrical two-dimensional mathematical model based on energy conservation equations was developed. The governing equations were discretized over finite volume controls using the enthalpy method and several numerical simulations were conducted to study multiple PCM/water heat exchangers behaviour. The impacts of the phase change material position and radius are experienced to evaluate the thermal performance of the heat exchanger. The optimal configuration for solidification is determined. It was found that, the heating time can be extended by properly moving the various phase change materials within the tube. Numerous cases are examined. The two cases that offer both advantageous heating choices have a heat delivery time to water that exceeds 138 minutes. When the impact of tube radius is examined, it is discovered that, in the case of a very thin PCM layer, the water records a high temperature of 60°C for 40 minutes before declining somewhat but staying above 42°C until t=56 minutes. For about 53 minutes, the water outlet temperature stays above 40°C when the phase change materials cylinder thickness reaches 17 mm. During the heat discharge, a comparatively improved heat evacuation capability is noted. Nevertheless, 28 kJ of heat are not utilized in total. The heat exchanger is unable to release the remaining energy.

Cite this article as: Oudaoui K, Faraji M. An in-depth numerical investigation of a solar latent heat storage unit incorporating phase change materials. J Ther Eng 2025;11(4):1023–1038.

***Corresponding author.**
*E-mail address: farajimustapha@yahoo.fr

This paper was recommended for publication in revised form by Editor-in-Chief Ahmet Selim Dalkılıç

Published by Yıldız Technical University Press, İstanbul, Turkey

INTRODUCTION

Due to economic progress and population growth, the world energy demand is continuously increasing [1]. Research into economical and clean energy options for water heating and cooling for domestic use has been a particular focus for decades [2]. Therefore, the use of renewable energy is promoted for its economic and ecologic viability. The share of electricity production should increase from 1.1% to 11.9% from 2015 to 2040. According to the Stated Policies Scenario, the world's need for electricity will increase at a rate of 2.1% year until 2040—double that of primary energy demand. As a result, in 2040, electricity will account for 24% of all final energy consumed, up from 19% in 2018. Growth in the demand for electricity is expected to be especially high in developing nations. In the Stated Policies Scenario, the share of low-carbon electricity sources will rise to 52% in 2040 as a result of market forces, government policies, and technological advancements [3]. One of the main problems associated with the use of renewable energy sources, except biomass, is its intermittent nature. This problem can be solved by storing part of the thermal energy during periods of maximum sun radiation and then using it during periods of low radiations or at night. In this regard, stored thermal energy is extracted and used in various applications, such as water heating, refrigeration and air conditioning. The use of thermal energy storage devices is therefore the most appropriate response: this solution helps to bridge the gap between energy supply and demand. Phase change materials (PCMs), which are used in solar latent heat storage units, are important components because of their high energy storage density and isothermal phase transition. The advantage of a system that includes PCM lies in its ease of use and consistent performance. However, when using PCMs, solar energy is stored as sensible and latent heat. The liquid and solid phases have different physical characteristics and are integrated into solar collectors. Therefore, the phase change process needs to be carefully analyzed to avoid any unmanageable situations in the actual operation of these devices. Ribezzo et al. [4] examined thermophysical properties and stability for various PCMs and they analyzed the most recent research on the use of additives and preparation techniques to improve liquid-to-solid PCMs for long-term heat storage applications. The following characteristics are required when choosing PCMs:

- A melting point that is appropriate for the purpose.
- High specific heat capacity and heat of fusion per unit weight and volume.
- Repeatable solidification/melting cycles without degradation are required for a PCM.
- A PCM should have a rapid rate of solidification development and a low degree of subcooling.
- A PCM should solidify and melts with little volume change.
- A low-cost PCM should be widely available.
- A PCM should not be poisonous, dangerous, or highly flammable.

Many recent papers offer current information on the utilization of PCMs in solar heating systems, such as buildings with low energy use, waste heat recovery, solar power plants, solar air heaters and electronic cooling [5]. Most PCMs generally have low thermal conductivity, which limits the thermal exchange between the heat transfer fluid and the storage medium. Therefore, designing an efficient and cost-effective heat storage system requires the development of technologies to improve thermal performance [6]. The thermal performance of solar water heaters through the integration of phase change materials (PCMs) was investigated by Al-Zurfi et al., [7]. Their research revealed that suitable PCMs can significantly boost the efficiency and heat retention of solar collectors, particularly during low radiation periods and after sunset. An optimal PCM configuration was used to maintain higher water temperatures for extended periods, thus prolonging the effectiveness of solar water heating into the evening hours. Seeniraj et al., [8] conducted a numerical study on a latent heat thermal storage (LHTS) module. The module shell contains the PCM, while the tubes carry the Heat Transfer Fluid (HTF). They investigated the impact of various geometric and thermophysical parameters on the performance of a LHTS unit. They noticed that a portion of the PCM at the exit of the HTF tube remained in a solid-state when using a tube without fins. An appreciable increase in energy storage was observed upon the inclusion of fins in the module. Akgün et al., [9] experimentally evaluated the fusion and solidification behaviors of PCMs in a vertical shell and tube heat exchanger. Their findings revealed a considerable decrease in fusion time with increasing HTF temperature. A lower mass flow rate of the HTF has resulted in reduced energy consumption. Other configurations of heat exchangers have been studied, such as that of Talebi et al., [10], which is a configuration of multiple PCMs. This study investigated the impact of three different angles as well as various values of the temperature and mass rate of heat transfer fluid during the charging and discharging phases. They found that the system configured with a 60 degree inclination angle demonstrated a 32.6% increase in the storage rate compared to 30 degree angle system. Additionally, elevating the HTF accelerates the phase-transition rates across both stages of the energy charging-discharging cycle. Similarly, Wang et al., [11] examined the discharge phase involving PCM within a plate-type heat exchanger. They highlighted that employing multiple PCMs greatly enhances temperature uniformity and overall discharge efficiency. Agyenim et al., [12] experimentally designed an energy storage system using Erythriol as a phase change material. The tests included systems without fins and two systems with circular and longitudinal fins. The results showed that the system with longitudinal fins gave the best results, with increased thermal response during the charging process. For the discharging process, they obtained reduced temperature gradients in the axial direction, supporting most models that neglect thermal conductivity in the axial direction. Abduljalil et al., [13] numerically investigated the solidification of a phase change material in a triplex exchanger tube. The heat transfer model used in the numerical simulation is pure conduction and natural convection. Different design parameters, such as the number of fins and the length and thickness of the fins, were considered. The findings highlight that the case with the 8-cell PCM unit geometry attained fast complete solidification, approximately 35% faster than that of the finned tube. The agreement of the results between the simulations and experiments shows that the finned geometry allows complete solidification in a short time. Furthermore, El Dessouky et al., [14] studied the effect of fluid inlet temperature, mass flow rate and flow direction on the temperature distribution. When the PCM melting time is completely reduced, the heat transfer coefficient of the PCM increases from the bottom of the vertical tube of the heat exchanger. In addition, increasing the water inlet temperature and mass flow rate decreases the PCM melting time. Wu et al., [15] introduced a novel model for latent thermal energy storage units (LTESU) and assessed its heat storage capabilities using three key measures: complete melting time, heat storage intensity, and storage amount. Factors affecting the model›s performance, including the PCM thermal conductivity, HTF inlet conditions, and fin geometry, are analyzed. The results indicate that a higher PCM thermal conductivity significantly reduces the thermal resistance, improving the storage performance. The HTF inlet velocity has a minimal impact, while higher HTF inlet temperatures notably enhance heat storage. Moreover, the effects of using PCM and PCM with nanotechnology as wallboard on a room›s thermal behavior were studied by Bahrami et al. [16]. According to their findings, compared to a standard room, the use of solid nanoparticles in PCM lowers the energy usage of the air conditioning system by 7.4%. The temperature fluctuation in the room is reduced by 52% and 31%, respectively, when utilizing nano-enhanced PCM, as opposed to conventional and pure PCM rooms. Also, Rajesh Akula et al., [17] introduced novel fin–Phase Change Material (PCM)–Expanded Graphite (EG) composite for better thermal management of a Li -ion battery at discharge rates higher than its maximum discharge limit. Fins and EG are augmented with PCM to enhance its effective thermal conductivity. They found that with the addition of 30% EG by volume, the maximum thermal performance of heat sink having 130 fins surpasses the heat sink having 260 fins filled with pure Eicosane by recording 1.5 °C lower temperatures for limit discharge rate. After reviewing the literature on brazed plate heat exchangers, Pulagam et al. [18] came to the conclusion that further study is necessary to create complete models that can incorporate a variety of geometric and flow characteristics. In order to fill in the existing research gaps, the authors suggest possible areas for further investigation. Gürtürk and Kok [19] noted that, depending on the application, the PCM solidification process and the energy release from the heat reservoir can differ. The first is that the thermal energy in the PCM should be delivered swiftly during PCM discharge, and it might be preferable to release the heat stored in the PCM more gradually. Due to the impact of subcooling during the solidification process, the energy held as latent heat in the PCM quickly discharges. Benbrika et al. [20] carried out a numerical analysis of the melting of elliptic systems with latent thermal energy storage. They look into how well it performs under various operating and design scenarios. They discovered that, in comparison to those of the vertical elliptic enclosure, the horizontal elliptic enclosure had a higher melting rate and, hence, a lower overall melting time. Rahimi et al., [21] performed an experimental study of PCM melting and solidification in a heat exchanger with fins. Their results demonstrated that using fins has a greater impact on the discharging process than on the charging process. The solidification rate of PCMs in shell-and-tube storage systems is much faster than that in rectangular configuration storage systems. Bouzennada et al., [22] numerically investigated the melting coupled free convection inside a finned enclosure and an empty enclosure. The heat transfer was enhanced by the heat distribution resulting from the addition of a fin inside PCM filled enclosure. The presence of a fin decreases the melting time by 13% and the thermal energy storage increases by 15%. Additionally, an experimental and computational investigation of internally finned tube heat exchangers was carried out by Pulagam et al. [23]. The shape of the fins is examined in terms of improving pressure drop and heat transfer. To help with the estimation of heat transfer and pressure drop characteristics on internally finned tube heat exchangers, a number of correlations have been developed. Pelella et al., [24] conducted a numerical analysis of a multi-source (air, solar, and ground) heat pump that incorporates a thermal energy storage system for heating residential spaces. The system was modeled using multiple sub-models taken into account for every component (heat exchangers, storage tanks, solar panels, compressors). Several cost scenarios in terms of incentives on investment costs and increased energy prices were analyzed. In the aforementioned studies, the heat exchangers contain either one PCM or two identical PCMs at most. No study has addressed the effect of the reallocations of multiple PCMs with different thermal properties within the tube on the thermal performance of the heat exchanger.

Numerous investigations in this field of expertise have been motivated by the growing demand for smaller heat exchangers that are more efficient. The majority of earlier research has concentrated on PCM charging or heat storage. However, important issues come up during discharge. How can we recover 100% of the stored energy if the phase change materials have low thermal conductivity? This is the main goal of the research. The proposed heat storage unit is particular in that it employs three distinct phase changes materials rather than just one. In order to maximize the latent heat storage unit›s discharge performance, these phase change materials are placed at various positions. The main purpose of the present paper is to study a Water/Multiple PCM heat exchangers with different PCM's thermal properties and to develop a mathematical model to analyze the effects of different key parameters able to enhance the discharge time. This involves an exploration of how different factors influence the thermal behavior of the proposed heat storage unit. The initial configuration of the PCM/water heat exchanger includes paraffin 53, n-eicosane $C_{20}H_{42}$ and Rubitherm paraffin PCMs. The subsequent configuration involves relocating these multiple PCMs to different positions within the tube. Also, the impact of the cylinder geometry and the thickness the PCMs layer were analyzed.

MATHEMATICAL MODEL

Physical Model

The heat storage unit, shown in Figure 1, consists of a coaxial tube filled with three PCMs with different melting temperatures. The outer tube is insulated. Herein, water plays the role of the HTF and flows inside the inner tube to carry out the heat stored in the PCMs. The hot water exits the heat exchanger from the outlet and extracts the thermal energy. The HTF enters at temperature less than the freezing point of all PCMs and provokes their solidification.

To simplify the mathematical model, the following assumptions were made:

- Axial conduction and viscous dissipation in the HTF are negligible.
- The effect of natural convection during melting is taken into account by using the effective thermal conductivity of the PCM liquid phase, Eq. (17).
- The thermophysical properties of the heat transfer fluid and the PCM are independent of temperature.
- The thermal resistance of the inner tube is negligible.

Mathematical modeling

The energy equation for the water is:

$$\frac{\partial \theta_f}{\partial t} = -A\frac{\partial \theta_f}{\partial x} - B\left(\theta_f - \theta^*\right) \tag{1}$$

where

$$\theta_f = T_f(x,t) - T_{m3}, \quad \theta^* = T\left(x, r = R_i, t\right) - T_{m3} \tag{2}$$

θ_f is fluid temperature at x position, and, θ^* is PCM temperature at x position and at interface water/PCM.

$$A = \frac{\dot{m}_f}{\rho_f \pi R_i^2}, \quad B = \frac{2U}{(\rho c_p)_f R_i}, \quad U = \frac{N_u\, k_f}{2R_i} \tag{3}$$

Herein, the first term on the left of equation (1) gives the sensible heat storage, the second term is the thermal gradient in the (ox) direction and the last term reflects the convective heat transfer between the water and the inner tube wall.

For phase change materials, the governing equations can be written as follows:

The sensible heat equation is:

$$h = h_m + \int_{T_m}^{T} \rho c_p dT \tag{4}$$

h_m is the enthalpy at the melting temperature, and c_p is the specific heat.

Therefore, the energy equation for the PCM is defined by:

$$\frac{\partial h}{\partial t} = \frac{\partial}{\partial x}\left(\alpha\frac{\partial h}{\partial x}\right) + \frac{1}{r}\frac{\partial}{\partial r}\left(\alpha\frac{\partial h}{\partial r}\right) - \rho_p \Delta H\frac{\partial f}{\partial t} \tag{5}$$

To solve the energy equation, Voller *et al.*, [25] proposed a numerical model using the enthalpy formulation. f represents the liquid fraction of the PCM and is given by:

$$f = 0, \quad T < T_m \; 0 < f < 1, \; T = T_m \; f = 1, \quad T > T_m \tag{6}$$

Additionally,

$$T_m = T_{m1}\, for \;\; 0 \le x \le \frac{L}{3}, \; T_m = T_{m2}\, for \; \frac{L}{3} \le x \le \frac{2L}{3}, \; T_m = T_{m3}\, for \; \frac{2L}{3} \le x \le L \tag{7}$$

Initial conditions

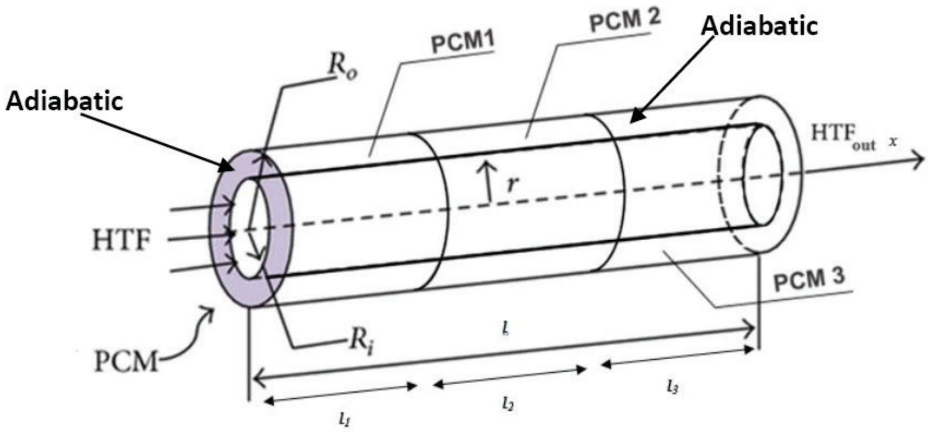

Figure 1. Coaxial heat exchanger with three PCM-filled tubes.

$$\theta_f(x,r,t=0) = T_i\text{-}T_{m3} \tag{8}$$

where

$i = 1 \quad 0 \le x \le \frac{L}{3},\ i = 2\text{: } \frac{L}{3} \le x \le \frac{2L}{3},$
$i = 3\text{: } \frac{2L}{3} \le x \le L\ ,\ \ L_1 = L_2 = L_3 = \frac{L}{3}$

Boundary conditions

The coaxial tube is insulated from the external surface, the inner fluid inlet velocity, u_0 and temperature, T_{f0} are kept constant and the monitored temperature at the outlet is $T_{f,out}$. The ends of the PCM in annulus tube are both insulated.

$$\frac{\partial T}{\partial x}\Big|_{x=0,r,t} = \frac{\partial T}{\partial x}\Big|_{x=L,r,t} = 0\ , \qquad R_i \le r \le R_0 \tag{9}$$

$$\frac{\partial T}{\partial x}\Big|_{x,r=R_0,t} = 0\,, \qquad 0 \le x \le L \tag{10}$$

-PCM/Water interface

$$-k\frac{\partial T}{\partial r}\Big|_{r=R_i,0<x<L} = B\left(\theta_f - \theta^*\right) \tag{11}$$

-PCM$_1$/PCM$_2$ interface

$$\begin{gathered} k_{pcm_1}\frac{\partial T}{\partial x}\Big|_{x=L/3^-,r} = k_{pcm_2}\frac{\partial T}{\partial x}\Big|_{x=L/3^+,r}\,, \\ T(L_1,r,t)_{PCM_1^-} = T(L_1,r,t)_{PCM_2^+} \end{gathered} \tag{12}$$

-PCM$_2$/PCM$_3$ interface

$$\begin{gathered} k_{pcm_2}\frac{\partial T}{\partial x}\Big|_{x=2L/3^-,r} = k_{pcm_3}\frac{\partial T}{\partial x}\Big|_{x=2L/3^+,r}\,, \\ T(L_2,r,t)_{PCM_2^-} = T(L_2,r,t)_{PCM_3^+} \end{gathered} \tag{13}$$

Thermo physical properties of a PCM are estimated as:

$$k_p = fk_e + (1-f)k_s \tag{14}$$

$$\rho c_p = f(\rho c_p)_l + (1\text{-}f)(\rho c_p)_s \tag{15}$$

The thermal conductivity of the PCM at the interfaces is estimated by:

$$k_l = \frac{k_+ k_-(\delta_- + \delta_+)}{k_+\delta_- + k_-\delta_+} \tag{16}$$

k_e *is* the effective thermal conductivity, which takes into consideration the natural convection in the liquid phase of the PCM, as follows [26,30]:

$$\frac{k_e}{k_l} = CRa^b \tag{17}$$

(C = 0.08, b = 0.25). Notably, the Rayleigh number R_a within each PCM tube compartment's depends on the thermo physical properties of PCM.

δ_+ is the distance between the interface and the first node of the material '+', and δ_- is the separation between the interface and the last node of the material '-'.

NUMERICAL METHOD

In this section, the focus was on the numerical method used to discretize the obtained algebraic equation with the boundary conditions. The control volume method described by Patankar [27] is introduced here, and the coupled energy equation was integrated with the control volume in the *(x,r)* plane. The control volume system is described in Figure 2.

The energy equation is integrated on the volume control as follows:

$$a_N\theta_N + a_W\theta_W + a_p\theta_p + a_E\theta_E + a_S\theta_S = b \tag{18}$$

With:

$$a_N = \frac{k_N r\Delta x}{\delta r_n},\ a_S = \frac{k_S r\Delta x}{\delta r_s},\ a_E = \frac{k_E r\Delta r}{\delta x_e},\ a_W = \frac{k_W r\Delta r}{\delta x_w} \tag{19}$$

$$b = (\rho c_p)_p r\frac{\Delta x\Delta r}{\Delta t}T_p^o + \rho_p\Delta H_p\frac{\Delta x\Delta r}{\Delta t}(f_p^o - f_p) \tag{20}$$

Eq.(18) becomes:

$$a_p = a_E + a_W + a_N + a_S + (\rho c_p)_p r\frac{\Delta x\Delta r}{\Delta t} \tag{21}$$

$$\delta x_E = x_E\text{-}x_p,\ \delta x_W = x_p\text{-}x_W,\ \delta r_N = r_N\text{-}r_p,\ \delta r_S = r_p\text{-}r_S \tag{22}$$

The solution to the equation for water is:

$$\left(\frac{1}{\Delta t} + \frac{A}{\Delta x} + B\right)\theta_f = \frac{\theta_{f,p}^o}{\Delta t} + \frac{A}{\Delta x}\theta_{f,w}^o + B\theta_f^o \tag{23}$$

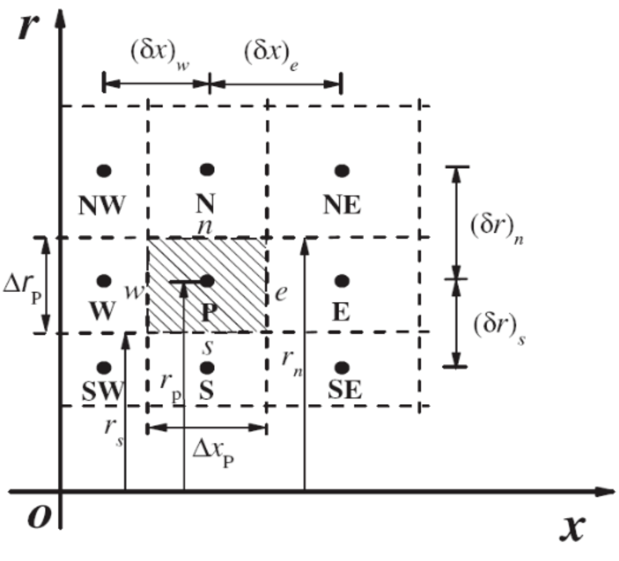

Figure 2. Control volume.

The central feature of the present fixed grid enthalpy method is the source term b. Here, hp and f refer to the enthalpy and the melt fraction, respectively, from the previous time-step. The source term b keeps track of the latent heat evolution, and its driving element is the melt fraction. Its value is determined iteratively from the solution of the enthalpy equation. Hence, after the $(n+1)^{th}$ numerical solution of the enthalpy equation of the P^{th} node, Eq. (18) may be rearranged as

$$a_p\theta_p = (\rho c_p)_p r\frac{\Delta x\Delta r}{\Delta t}T_p^{old} + \rho_p\Delta H_p\frac{\Delta x\Delta r}{\Delta t}(f_p^o - f_p^n) - (a_N\theta_N + a_W\theta_W + a_E\theta_E + a_S\theta_S) \tag{24}$$

If phase change is occurring about the P^{th} node (i.e., $0 < f < l$), the $(n+1)^{th}$ estimate of the melt fraction needs to be updated such that the left side of Eq. (18) is zero

$$0 = (\rho c_p)_p r\frac{\Delta x\Delta r}{\Delta t}T_p^{old} + \rho_p\Delta H_p\frac{\Delta x\Delta r}{\Delta t}(f_p^o - f_p^{n+1}) - (a_N\theta_N + a_W\theta_W + a_E\theta_E + a_S\theta_S) \tag{25}$$

hence, by subtracting Eq. (25) from Eq. (24), the new melt fraction is

$$f_p^{n+1} = f_p^n + \frac{\Delta t}{\Delta x\Delta r}\frac{a_p}{\rho_p\Delta H_p}\ a_p\theta_p \tag{26}$$

The melt fraction update Eq. (27) is applied at every node after the $(n+1)^{th}$ solution of Eq. (26) for sensible volumetric enthalpy h, along with under/over shoot corrections:

$$if\ \ f_p^{n+1} < 0:\ f_p = 0,\ \ if\ \ f_p^{n+1} > 1:\ f_p = 1 \tag{27}$$

The Tri Diagonal Matrix Algorithm (TDMA) is used to solve the algebraic equation system, and implemented in program code using FORTRAN language for numerical simulation.

Mesh and Time Step Optimization

The algorithm implemented in a personal FORTRAN code is used to solve the obtained algebraic equations. The transient thermal behavior of the PCM heat exchanger was simulated under different conditions during the discharge process. In order to achieve the accuracy of the numerical results, several numerical simulations were conducted to analyze the impact of the mesh size and the time step. Table 1a and 1b indicate that, for the time step Δt=60 s, varying the mesh size from nxm= (120x60) to (140x70) results in a relative deviations in the outlet water temperature $T_{f,out}$ and the liquid fraction f, below 0.057% and 0.259%, respectively. Also, for the mesh size nxm=(120x60), changing the time step from Δt=60 s to 40 s generates relative deviation of less than 0.28% and 0.77% for temperature $T_{f,out}$ and liquid fraction f, respectively. Notably, other time steps and mesh sizes were tested, but they require lengthy calculation times without significant changes in the outcomes.

Convergence

Iterative calculations are necessary due to the coupling and nonlinearity of the governing equations. When the following requirement is satisfied, the calculation converges:

$$\frac{\sum_i |\theta^{k+1}(i) - \theta^k(i)|}{\sum_i |\theta^k(i)|} < \varepsilon_k \ \text{and}\ \frac{\sum_i |f^{k+1}(i) - f^k(i)|}{\sum_i |f^k(i)|} < \varepsilon_f \tag{28}$$

where$f^k(i)$ is the liquid fraction and $\theta^k(i)$ is the temperature at node (i) at iteration k. The parameter ε must be small enough ($\varepsilon_\theta = 10^{-5}$, $\varepsilon_f = 10^{-3}$).

Validation

The mathematical model was validated by comparing it to experimental data previously published by Lacroix [28]. The experience involves a water/PCM shell and tube latent heat storage unit consisting of two concentric cylindrical pipes, with a single PCM (n-octadecane) filling the shell space and hot water flowing through the inner tube. The experimental setup contains several components including a heat storage container, a high temperature bath, a low temperature bath, circulation pumps, N-type thermocouples, a data acquisition unit and a piping system. The charge

Table 1. Effect of the mesh size (a) and time step (b)

nxm	CPU(hours)	T (°C)	Deviation (%)	f	Deviation (%)
80x40	06:55	30.06	-	0.398	-
100x50	08:25	31.3	4.125	0.389	2.261
120x60	09:40	31.542	0.773	0.386	0.771
140x70	12:26	31.56	0.057	0.385	0.259

(a, Δt =60 s)

Δt	CPU(hours)	T (°C)	Deviation (%)	f	Deviation (%)
80 s	06:00	29.018	-	0.378	-
60 s	08:15	31.542	8.69	0.386	2.11
40 s	10:26	31.632	0.28	0.389	0.77

(b, nxm=120x60)

of the PCM is studied experimentally for water (HTF) inlet temperatures $T_{f,in}$ = 38°C, mass flow rate was maintained constant during the experimental test to a value of 0.0315 kg/s. Table 2 summarizes the thermal properties of the HTF and PCM (n-octadecane). The length, inner and outer radii of the tube are L =1 m, R_i =1.27 cm and R_o =2.58 cm, respectively. Thermocouple is used to measure temperature at location x = 0.5 m in the inner tube.

Figure 3 provides a comparison between variation of numerical and experimental temperatures. As can be seen in this figure, a good agreement between the predicted and experimental results is observed with minor differences. At the end of the melting process, the water numerical temperature equals 38 °C and that of the experiment is about 37 °C, the reason for this can be revealed to the measurements uncertainties or to the heat lost from the PCM tube to the surrounding due to the material used for thermal insulation of the experimental setup. Therefore, the present computational model can be accurately used for the study of the proposed latent heat storage unit using three phase change materials, with different melting temperatures.

In the following section, several numerical simulations were conducted according to the subsequent the steps:

- Collect of required input data for computer runs: PCM properties, heat exchanger geometry and environmental data,
- Optimization of mesh size and time step for result accuracy,
- validation with previous published experimental results,
- Delving a parametric study to depict the effect of various key parameters on the thermal performances of the proposed latent storage system,
- Analyzing the optimal configuration and recommendations.

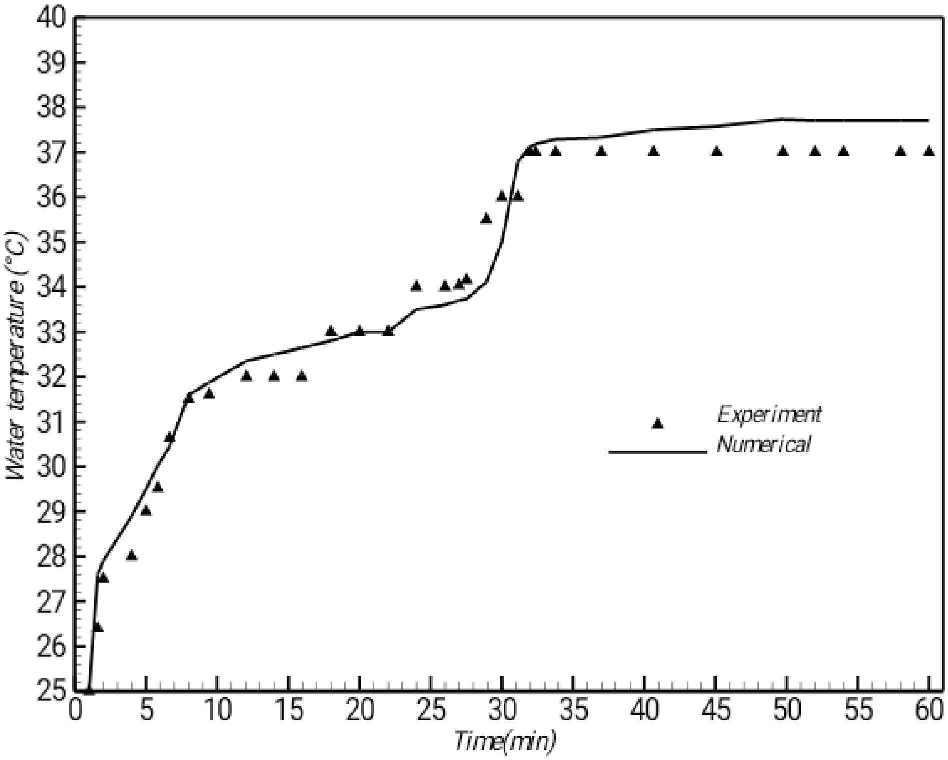

Figure 3. Comparison of measured [28] and numerical temperatures as a function of time at location x = 0.5 m. (created by author).

Table 2. Thermo physical properties for experience [28]

Material		*Tm* (°C)	*ΔH*(kJ/kg)	*cp* (kJ/kg. K)	*ρ* (kg/m³)	*k* (W/m².°C)
n-octadecane	S	27.7	243.5	2.22	771	0.148
	L					0.356
Water		-	-	4.178	995	0.62

RESULTS AND DISCUSSION

The heat exchanger is initially filled with three different PCMs in the liquid state. The inlet water temperature is $T_{f,in}$ = 25°C. Cold water flows through the inner pipe and extracts heat from multiple PCMs. PCM in contact with the cold water cools, and when its temperature drops to the freezing point it begins to solidify. The process continues until all the multiple PCMs are discharged (solidified). In the present paragraph the performance of the solidification process is investigated. Different control parameters, such as liquid fraction, outlet water temperature, sensible and latent heat efficiency, overall discharge time and PCM thickness effect are analyzed.

Base Case Analysis

Before presenting the results, we analyze the basic configuration. Three PCM are arranged from the left to the right side as follows: PCM_1: Rubitherm Paraffin, PCM_2: Paraffin 53 followed by PCM_3: N-eicosane $C_{20}H_{42}$. The HTF mass flow rate $\dot{m}_f$ and the inlet temperature $T_{f,in}$ are 0.160 kg/s and 25°C, respectively. The proposed heat exchanger can be used for residential purposes. The proposed PCM water heat exchanger has a mass flow of 0.16 kg/s equivalent to one bucket (10 L) of hot water every minute, and its size depend on the building type and number of occupants.

It should be noted that paraffinic phase change materials are mostly chemical products. They have the following benefits: low subcooling, no corrosion, less evident phase change separation, strong chemical stability, low cost, and good solid formability. Also, The paraffin-based PCMs utilized in this work are economically advantageous to integrate into the current heat storage system for passive water heating because coaxial tube heat exchanger technology is well-developed. The properties of different materials are

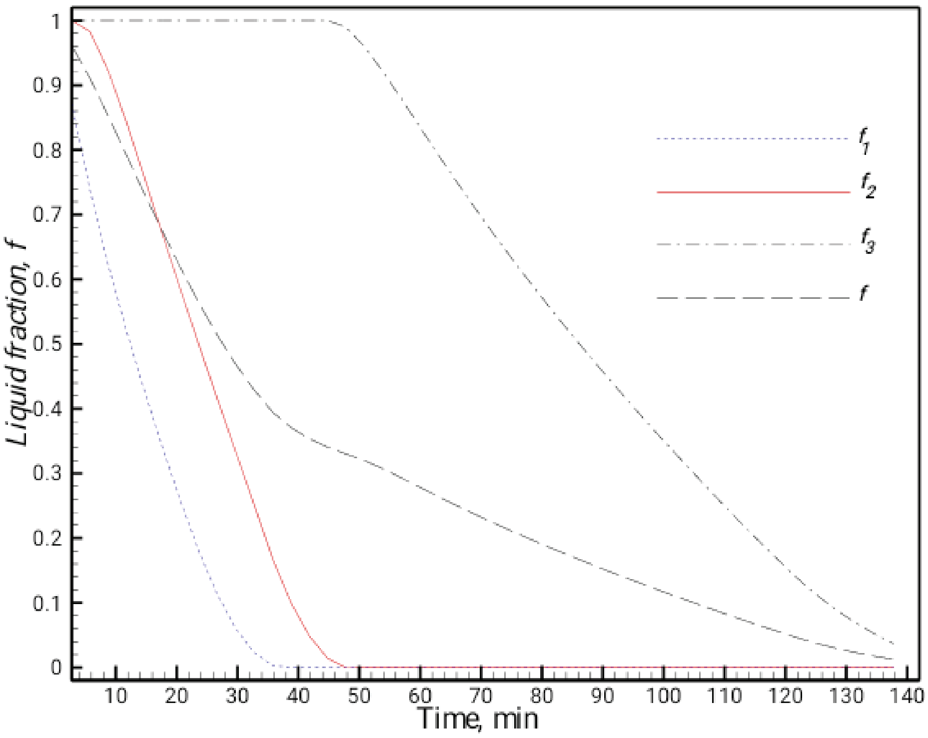

Figure 4. Time progression of the PCM liquid fraction.

Table 3. Thermophysical properties [29]

Material		*Tm* (°C)	*ΔH*(kJ/kg)	*cp* (kJ/kg. K)	*ρ* (kg/m³)	*k* (W/m².°C)
PCM_1:	S	60.0	214.0	0.812	930	0.20
Rubitherm Paraffin	L					0.21
PCM_2:	S	53.0	164.0	2.385	830	0.28
Paraffin 53	L					0.19
PCM_3:	S	36.5	237.4	2.050	800	0.16
N-eicosane $C_{20}H_{42}$	L					0.21

given in Table 3, and the dimensions of the storage unit are as follows: L_1=L_2=L_3= 0.333 m, interior and exterior tube radii are R_i= 0.0075 m and R_0=0.015 m, respectively. The heat transfer fluid to be heated comes into contact with the PCM, holding the stored thermal energy. As the PCM cools, it undergoes a phase change from the liquid to the solid state. Latent heat is released during this phase change, providing a constant temperature near the solid/liquid interface until complete solidification of the PCM.

Figure 4 shows the time progression of the liquid fraction within the three compartments and the variation of the corresponding total liquid fraction. The liquid PCM inside the tube near the cold water releases its thermal energy. When the temperature of each PCM reaches the freezing point, solidification initiates. The full solidification of PCM_1 occurs rapidly after approximately 35 min; in contrast, second compartment, PCM_2, takes approximately 47 minutes to freeze. The third PCM solidifies slowly and the liquid phase is exhausted after 137 minutes. Note that thermal resistance increases with increasing solidification fraction of the PCM_3. Therefore, the solidification rate decreased with time and the slope of the total liquid fraction *f* curve is between the slopes of PCM_1 and PCM_2 curves, as can be seen in Figure 4.

Figure 5 is used to monitor the time variation of the average temperature inside each PCM compartment. During the first five minutes, PCM_1, with freezing temperature 60°C, cools the first followed by PCM_2 and then by PCM_3. Between 5 and 10 minutes of discharge, PCM_2 cools faster compared to other PCMs. For time greater than 20 minutes, PCM_3 cools more than other PCMs. The slop of all curves changes in intensity when phase change process initiates within different compartment. After a net decrease in temperature during the solidification, average temperature become near constant, it's the full solidification of PCM. Note that compartment 3 remains warmer during a long period and PCM_3 average temperature stays between 35 and 30°C during more than 80 minutes. Average temperature of PCM_1 and PCM_2 drops to 25°C from 70 minutes to the end of the discharge process.

The time progression of the HTF outlet temperature during the solidification process is displayed in Figure 6. The HTF outlet temperature continuously drops throughout the discharge process. The water shows a higher thermal gradient at the start of the discharge process, and as time progresses, the inner tube surface begins to cool; therefore, a layer of solid PCM recovers it. The solid layer builds quickly, the thermal resistance between the liquid PCM and HTF increases, and with no convective heat transfer occurs in the solid layer. As a result, the HTF outlet temperature decreases. The reduced PCM heat conductivity combined with the free convection cancelation are what cause this result. The PCMs used are characterized by different thermophysical properties, especially their melting temperature. The change in the shape of the *T* curves from convex to concave is essentially due to the end of the solidification process of one PCM. Especially, after 35 minutes, the *T* curve passed from concave to convex, indicating the end of the solidification of PCM_1. At t =45 min, the shape changes from convex to concave due to the full solidification of the PCM_2 compartment, according to Figure 6. The HTF output temperature approaches the inlet temperature at full solidification, indicating the exhaustion of all the useful energy.

Table 4. Water-PCM heat exchanger specifications

Parameter	Value
External radius of tube	R_0 = 1.5 cm
Internal radius of tube	R_i = 0.75 cm
Total length of the tube	L = 1 m

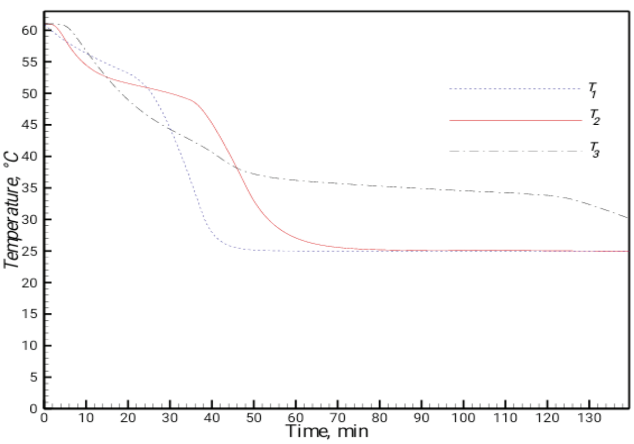

Figure 5. Time variation of mean temperature of multiple PCMs.

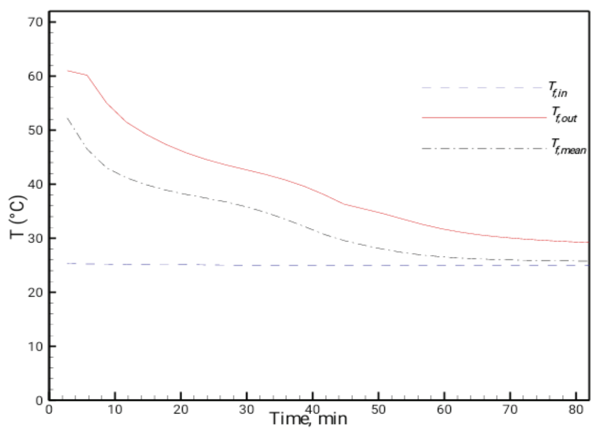

Figure 6. Temporal variations of inlet,outlet and average water temperatures.

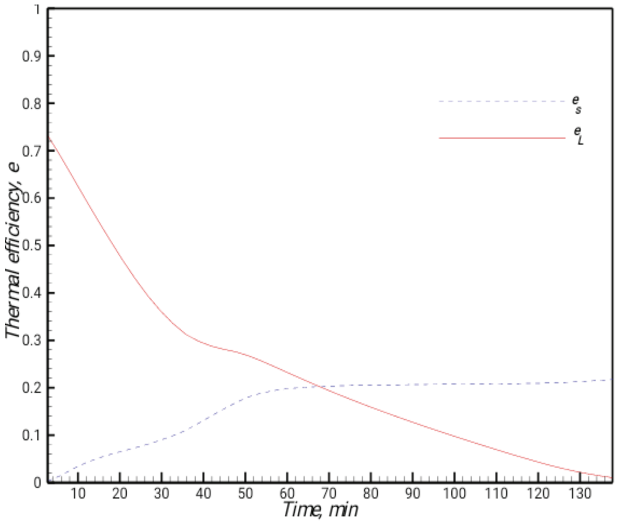

Figure 7. Time wise variation in the thermal storage efficiency during the solidification process.

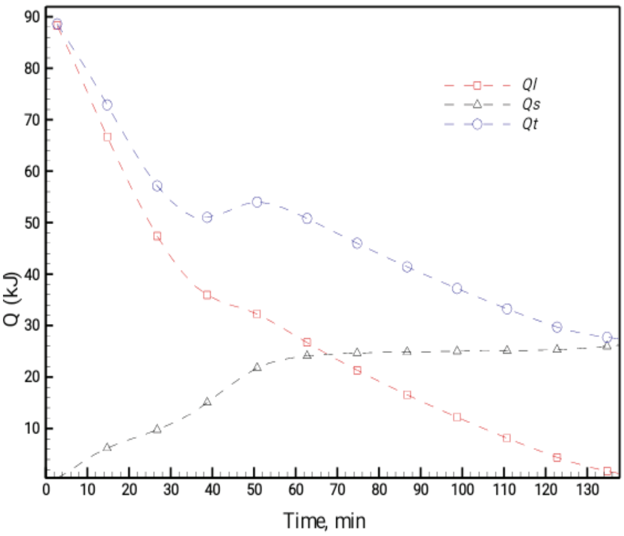

Figure 8. Latent, sensible and total energy available and stored in the PCMs within the heat exchanger.

Figure 7 shows the temporal variation in the heat storage efficiency during the discharge process. When PCM starts to solidify, its temperature remains relatively constant and releases its latent heat of fusion. Sensible heating of the PCM is present and rises from the beginning to 35 minutes. Water, inside the tube, partially loses heat in the PCM compartments and the sensible efficiency e_s increases, while the latent efficiency e_L remains quasi constant between 35 and 50 minutes. The next step is characterized by a smooth decrease in e_L and a pseudo constant sensible heat efficiency, $e_{s,}$ until the end of the discharging process. Note that, at this point, the three PCMs are entirely solid, and approximately, 21% of the energy is not used and any further heat transfer is a sensible heating, leading to lower energy storage efficiency at the end of the discharge process.

Figure 8 represents the energy available and stored in the PCM tube. The total latent heat is exhausted quickly. This energy is absorbed by the water. Analysis of the energy variations in the water/PCM heat exchanger clearly shows that the sensible heat, Q_s, absorbed by the PCM is positive and increases when the discharging process is running. The sensible heating of the PCM increases since the launch of the water/PCM heat exchange. The increase in the sensible heat accelerates after the total solidification of PCM_1, especially at the level of the convex part of the curve of the total heat $Q_{T,}$ which rapidly increases from t=35 min to 50 min, with a sensible intensification after the total solidification of PCM_1. Therefore, instead of heating the water at the outlet, some of the heat is unfortunately drifted and trapped in the PCM. The heat transfer increases toward the water, and the total heat available in the PCM, Q_T, reaches a maximum value of 54 kJ at t = 50 min. Outlet water temperature equals 35°C. As time progresses, PCM solidify and it temperature decreases due to the continuous flow of cold water. The preheated water removes increasingly less heat from the PCMs due to the decrease in the temperature difference between the water and the PCM. This behavior leads to the collapse of the thermal gradient, which causes a reduction in the Q_T value with time, as shown in Figure 8. A relatively better heat evacuation capacity Q_T during all useful discharge stages is observed. A total of 28 kJ of heat is not used. That residual energy cannot be extracted from the heat exchanger. Note that, the stored energy depends on the subcooling of the solid phase. Sensible heat is stored in the solid and when the temperature of the solid pcm reaches the melting point it melts and latent heat storage begins.

Effect of PCM Relocation

The majority of the energy is kept in latent heat by the phase change mechanism in energy storage devices that employ PCMs. The heat is transferred to or from the PCMs by melting or solidification, depending on the tube and calendar temperatures. It is crucial to research the significance of the second process, the solidification or discharge of the PCM. The cold water's capacity to extract the most latent heat from the PCM during solidification in the allotted time is the subject of the parametric study. Figure 9 shows four cases under study, involving replacing phase change materials at different locations in the tube and examining how they affect the heat discharge efficiency, which is the subject of the present section.

Figure 10 shows the time progression of the liquid fraction according to the four cases studied. The fundamental setup, case (a), was discussed in the above section. Analysis of that figure shows that case (c) offers the fastest discharge option with 92 minutes of full solidification. Cases (a) and (d) present both favorable heating options with a longer delivery of heat to water exceeding 138 minutes. Note that the discharge process clearly depends on the PCMs reallocation, and the solidification is gradual. Throughout the

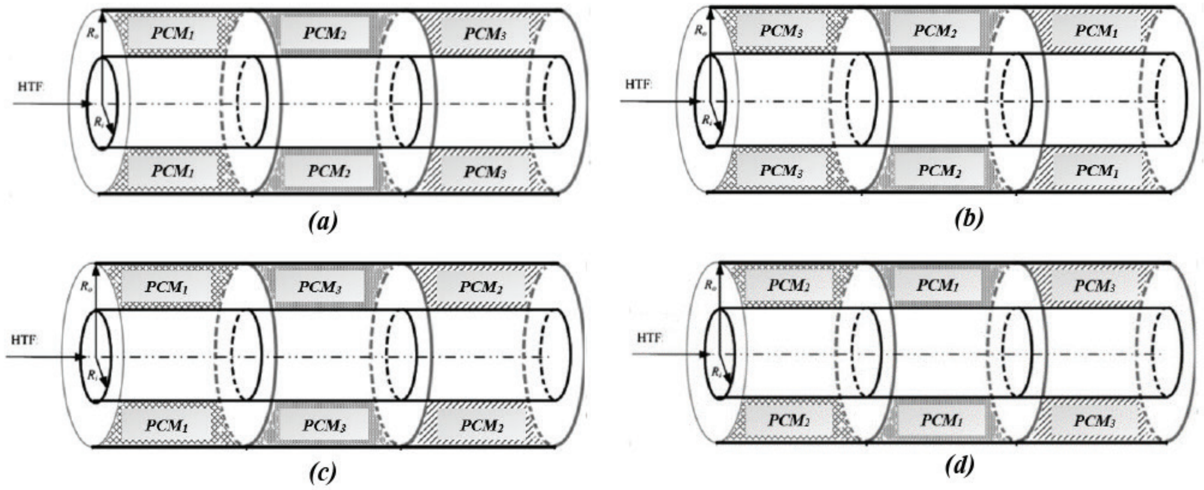

Figure 9. Cases under study.

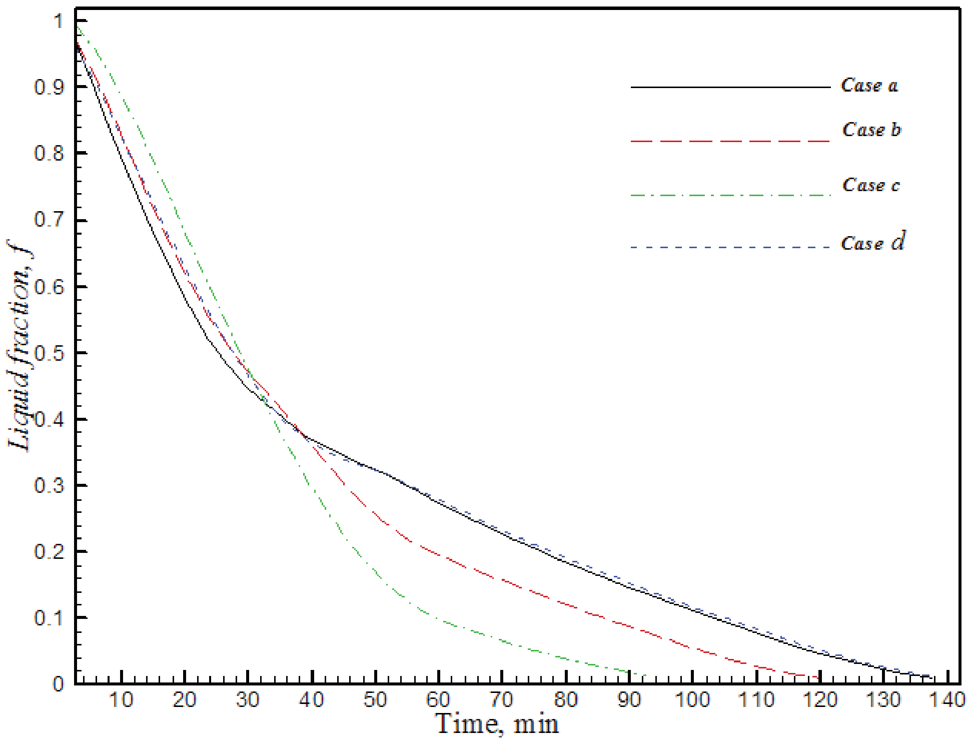

Figure 10. Time progression of the liquid fraction for the four cases.

discharge time of 1 hour, 73% of the PCM solidifies for base case (a), and approximately 80% is found in the solid-state for case (b). Ninety percent of the liquid PCM is exhausted for case (c). The discharge process is much slower in case (d), as in the basic configuration, case (a).

Figure 11 illustrates the temporal evolution of the outlet water temperature according to the studied cases. Analysis of that figure shows that, during 67 minutes, case (c) offers a good heating option with the greatest temperature, resulting in a good heat extraction. However, the liquid PCM is consumed quickly in 92 minutes. In case (b), the water is well heated and only 120 minutes are necessary for the PCM to fully solidify. Finally, case (a) and case (d) offer both a longer heating period but with 4°C less than that of the other cases. Upon comparing the four studied cases, it is remarkable that the temperatures are approximately uniform after 70 minutes to the end where all studied cases show the same behavior.

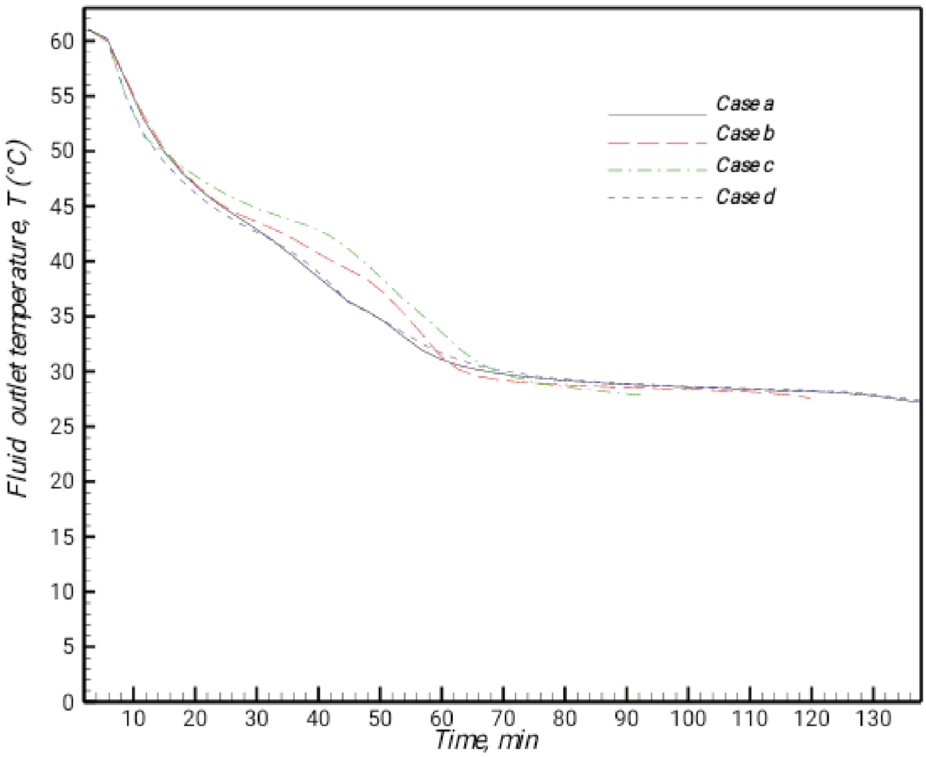

Figure 11. Time wise variation in the water outlet temperature for the four cases.

Effect of The PCM Tube Radius

The thickness of a PCM plays a crucial role in the thermal performance of the heat exchangers. A thinner PCM layer can lead to faster solidification. This can improve the discharge time, but it can reduce the total amount of energy stored or released. A thicker PCM layer stores more energy, but it can also slow the phase change process, thereby, extending the discharge time. Several numerical simulations are conducted, the mass of the PCM is kept constant at m_0= 0.450 kg. Note that, when the thickness of the PCM is reduced, the length of the cylinder increases. Five values of the radius R_0 are tested: R_0= 11 mm, 13 mm, 15 mm, 16 mm and 17 mm. PCM thickness is (R_0 – R_i) and depends to the cylinder length for PCM mass held constant. Consequently, the passage from the PCM cylinder radius R_0 to $R_{0.1}$ results in variations in the tube length from L to L_1, according to Table 5.

Table 5. Cylinder Length versus Radius

$R_{0.1}$(m)	L_1(m)
0.011	2.60
0.013	1.50
0.015	1.00
0.016	0.85
0.017	0.73

In the above subsection, it was found that case (c) provides a prompt discharge time offering, relatively, good water heating and less sensible PCM reheating. In the present section, the PCM cylinder radius R_o for case (c) is varied to elucidate its impact on the overall heat exchanger heating performance.

Figure 12 shows the temporal evolution of the water temperature at the outlet of the PCM/water heat exchanger for the different values of the PCM cylinder radius. Analysis of this figure shows that for a very thin PCM layer (11 mm), the outlet water registers a high temperature of 60°C for 40 minutes, and then it temperature decreases but remains above 42°C until t= 56 min. When the thickness of the PCM cylinder increases to 17 mm, the water outlet temperature generally goes through two stages: the steady-state heating stage, where $T_{f,out}$= 40°C for approximately 53 minutes, followed by a decrease to 28°C, until t=80 min. Furthermore, no temperature variations for the remaining stage. For larger PCM radius, the length of the heat exchanger tube decreases, according to Table 5 and the water temperature decreases faster. In fact, when the radius of the PCM tube is thick, and with the problem of low thermal conductivity of the PCM, during discharge, a layer of solid PCM is formed on the outer surface of the inner tube and, over time, the thickness of this layer increases and amplifies the thermal resistance between the water and the hot liquid PCM. Therefore, the cold water entering the inner tube extracts less heat and leaves the heat exchanger with a low temperature.

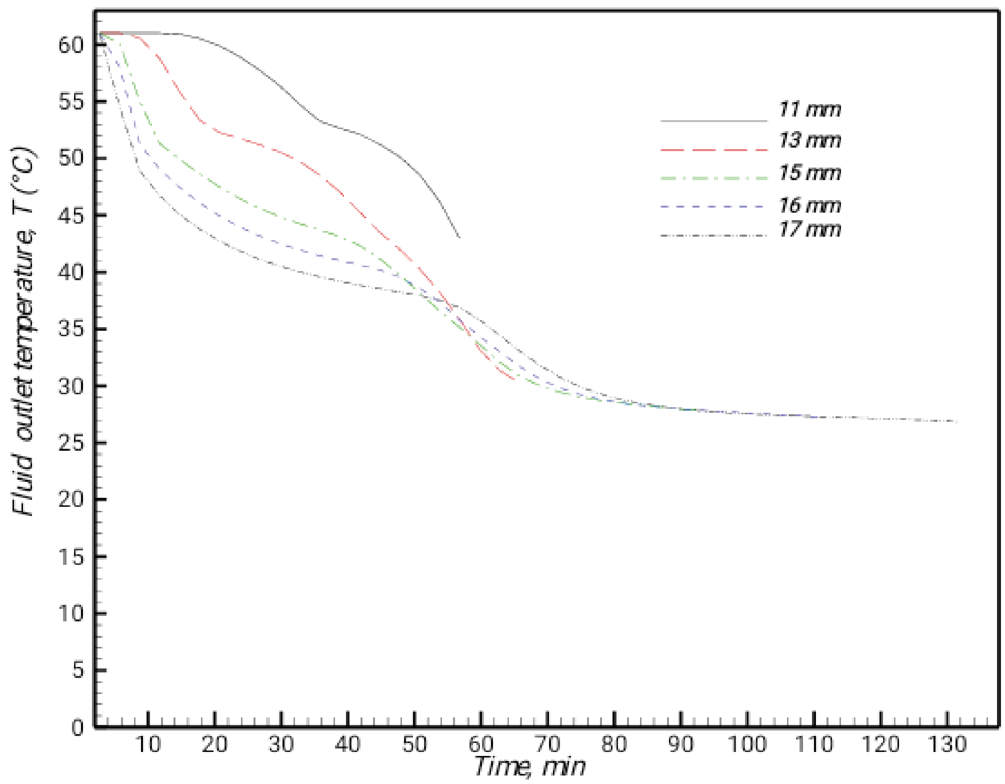

Figure 12. Temporal evolution of water temperature at the outlet of the heat exchanger for different PCM radii.

Table 6. Effect of PCM radius on heat exchanger performances

PCM radius	Tf,out (°C) (at 20 min)	Tf,out (°C) (at 50 min)	Total extracted heat by water (kJ)	Full solidification time (min)
11 mm	60	50	175	56
13 mm	52	40	152	66
15 mm	47	38	140	93
16 mm	45	39	137	110
17 mm	42	38	134	131

When the thickness of the PCM is relatively small (R_0=11 mm), the length of the tube increases and heat exchange surface, between the water and PCM, increases. This promotes a faster extraction of latent and sensible heat stored in the heat exchanger. Table 6 shows that the intensity of heat removal from the water/PCM heat exchanger is significantly greater for the R_0=11 mm than for R_0=17 mm case. Indeed, after 56 minutes of discharge, the amount of water extracted heat was 175 kJ compared to 134 kJ for a thickness of 17 mm. Note that for all PCM radii, a residual amount of the stored energy remains unused in the water and PCM inside the heat exchanger. Additionally, according to the results summarized in Table 6, the heating behavior of water is monitored by the PCM solidification rate, which depends on the tube geometry and PCM thermal properties in different tubes compartments, mainly the latent heat of fusion of the PCMs (ΔH_1 = 164 kJ/kg, ΔH_2 = 216 kJ/kg, ΔH_3 = 234,4 kJ/kg).

CONCLUSION

The thermal discharge performance of a PCM/water heat exchanger was studied numerically. Three different phase change materials, Paraffin 53, Rubitherm Paraffin and n-eicosane $C_{20}H_{42}$ were used. A mathematical model was developed to analyze the thermal behavior and performance of the proposed latent heat storage unit. After identifying the geometry and operating parameters, the energy conservation equations were integrated using the finite volume control method. Several numerical simulations were performed to study the impact of the operating parameters of this novel storage system. It can be concluded that the improvement in the solidification process is significant due to the different thermophysical properties of the phase change materials. As time progresses, the phase change materials undergo solidification, and the rate of heat evacuation depends on the heat exchanger configuration. After approximately 138 minutes, 85% of the phase change materials solidified. Free convection and conduction heat transfer modes are activated during the phase change process. Three phase change materials are located at four different locations, and the impact of PCM relocation is examined. Placing the phase change material with the lowest melting temperature at the tube inlet accelerates the solidification process. Furthermore, the most ideal configuration is determined. Finally, conserving the same phase change materials mass, the phase change materials thickness deeply influences the PCM/water heat exchanger performance. It was found that:

- The position of the phase change materials and its thermal characteristics affect its complete solidification. As the PCM solidifies more, thermal resistance rises, and as time passes, the rate of heat discharge falls.
- The water exhibits a greater thermal gradient at the beginning of the discharge process, and as the process goes on, the inner tube surface cools. The solid layer forms fast, increasing the thermal resistance between the liquid phase change material and heat transfer fluid, which lowers the temperature of the water outlet.
- The phase change material absorbs a positive quantity of sensible heat, which rises as the discharging process proceeds. Some heat has drifted and become trapped in the phase change materials.
- As the temperature differential between the water and the phase change materials decreases, the preheated water extracts progressively less heat from the phase change materials. This behavior causes the PCM/Water thermal gradient to collapse.
- Upon comparing the four phase change materials reallocation cases, it is remarkable that the temperatures are approximately uniform after 70 minutes to the end where all studied cases show the same behavior.

For a careful design of phase change materials heat storage systems, appropriate phase change materials choices combined with well-considered tube geometries are necessary. As future research work and for passive heating using solar energy, the PCM/Water heat exchanger will be connected to a solar collector in different climatic regions in Morocco to analyze its dynamic behavior.

NOMENCLATURE

c_p	specific heat (kJ/kgK)
f	liquid fraction
h	specific enthalpy (kJ/kg)
HTF	heat transfer fluid or water
k	thermal conductivity (W/m K)
L	length of the tube (m)
m	mass of the PCM (kg)
Nu	Nusselt number
Q	heat transfer rate (W)
r	radial coordinate (m)
R	Radius (m)
Ra	Rayleigh number
R_i	internal radius of the tube (m)
R_o	external radius of the tube (m)
T	temperature (°C)
t	time (s)
U	convective heat transfer coefficient (W/m²°C)
x	axial coordinate

Greek symbols

α	thermal diffusivity (m²/s)
Δr	radial space step (m)
Δx	axial space step (m)
Δh	latent heat of fusion (kJ/kg)
ρ	density (kg/m³)

Subscripts

1,2,3	PCM_1, PCM_2, PCM_3
e	east node
E,W,N,S	east, oust, north, south control volumes
f	heat transfer fluid
i	inlet , internal tube, initial or interface
in	inlet
l	liquid phase or latent
m	melting
o	outlet
out	outlet/external tube
P	central node
s	solid phase, sensible heat or south node
t	Total

AUTHORSHIP CONTRIBUTIONS

Authors equally contributed to this work.

DATA AVAILABILITY STATEMENT

The authors confirm that the data that supports the findings of this study are available within the article. Raw data that support the finding of this study are available from the corresponding author, upon reasonable request.

CONFLICT OF INTEREST

The author declared no potential conflicts of interest with respect to the research, authorship, and/or publication of this article.

ETHICS

There are no ethical issues with the publication of this manuscript.

STATEMENT ON THE USE OF ARTIFICIAL INTELLIGENCE

Artificial intelligence was not used in the preparation of the article.

REFERENCES

[1] Al Shawa B. An equitable energy allowance for all: Pathways for a below 2 °C-compliant global buildings sector. Energy Rep 2022;8:15377−15398. [CrossRef]
[2] Dey B, Misra S, Garcia Marquez FP. Microgrid system energy management with demand response program for clean and economical operation. Appl Energy 2023;334:120717. [CrossRef]
[3] Nassar NT, Wilburn DR, Goonan TG. Byproduct metal requirements for U.S. wind and solar photovoltaic electricity generation up to the year 2040 under various Clean Power Plan scenarios. Appl Energy 2016;183:1209−1226. [CrossRef]
[4] Ribezzo A, Falciani G, Bergamasco L, Fasano M, Chiavazzo E. An overview on the use of additives and preparation procedure in phase change materials for thermal energy storage with a focus on long term applications. J Energy Storage 2022;53:105140. [CrossRef]
[5] Anilkumar BC, Maniyeri R, Anish S. Optimum selection of phase change material for solar box cooker integrated with thermal energy storage unit using multi-criteria decision-making technique. J Energy Storage 2021;40:102807. [CrossRef]
[6] Ghosh D, Ghose J, Datta P, Kumari P, Paul S. Strategies for phase change material application in latent heat thermal energy storage enhancement: Status and prospect. J Energy Storage 2022;53:105179. [CrossRef]
[7] Al-Zurfi HA, Talib MA, Hassan QH, Aljabri GJ. A numerical study to improve the efficiency of solar collector used for water heating using phase change material. J Adv Res Numer Heat Transf 2024;17:1−13. [CrossRef]
[8] Seeniraj RV, Velraj R, Narasimhan NL. Thermal analysis of a finned-tube LHTS module for a solar dynamic power system. Heat Mass Transf 2002;38:409−417. [CrossRef]
[9] Akgün M, Aydın O, Kaygusuz K. Experimental study on melting/solidification characteristics of a paraffin as PCM. Energy Convers Manag 2007;48:669−678. [CrossRef]
[10] Talebizadeh Sardari P, Mahdi JM, Mohammed HI, Moghimi MA, Eisapour AH, Ghalambaz M. Consecutive charging and discharging of a PCM-based plate heat exchanger with zigzag configuration. Appl Therm Eng 2021;193:116970. [CrossRef]
[11] Wang P, Li D, Huang Y, Zheng X, Wang Y, Peng Z, et al. Numerical study of solidification in a plate heat exchange device with a zigzag configuration containing multiple phase-change-materials. Energies 2016;9:394. [CrossRef]
[12] Agyenim F, Eames PC, Smyth M. A comparison of heat transfer enhancement in a medium temperature thermal energy storage heat exchanger using fins. Sol Energy 2009;83:1509−1520. [CrossRef]
[13] Al-Abidi AA, Mat S, Sopian K, Sulaiman MY, Mohammad AT. Numerical study of PCM solidification in a triplex tube heat exchanger with internal and external fins. Int J Heat Mass Transf 2013;61:684−695. [CrossRef]
[14] El-Dessouky H, Al-Juwayhel F. Effectiveness of a thermal energy storage system using phase-change materials. Energy Convers Manag 1997;38:601−617. [CrossRef]
[15] Wu Y, Li D, Jiang W, Zhu S, Zhao X, Arıcı M, et al. Energy storage and exergy efficiency analysis of a shell and tube latent thermal energy storage unit with non-uniform length and distributed fins. Sustain Energy Technol Assess 2022;53:102362. [CrossRef]
[16] Nguyen Trung K. The temperature distribution of the wet cylinder liner of V-12 engine according to calculation and experiment. J Therm Eng 2021;7:1872−1884. [CrossRef]
[17] Akula R, Balaji C. Thermal management of 18650 Li-ion battery using novel fins–PCM–EG composite heat sinks. Appl Energy 2022;316:119048. [CrossRef]
[18] Pulagam MK, Rout SK, Sarangi SK. A state-of-the-art review on thermo fluid performance of brazed plate heat exchanger for HVAC application. J Therm Eng 2024;10:1390−1410. [CrossRef]
[19] Gürtürk M, Kok B. A new approach in the design of heat transfer fin for melting and solidification of PCM. Int J Heat Mass Transf 2020;153:119671. [CrossRef]
[20] Benbrika M, Teggar M, Benbelhout M, Ismail KAR, Bouabdallah S. Effect of orientation of elliptic tube on the total melting time of latent thermal energy storage systems. J Therm Eng 2021;7:1479−1488. [CrossRef]
[21] Rahimi M, Ranjbar AA, Ganji DD, Sedighi K, Hosseini MJ, Bahrampoury R. Analysis of geometrical and operational parameters of PCM in a fin and tube heat exchanger. Int Commun Heat Mass Transf 2014;53:109−115. [CrossRef]
[22] Bouzennada T, Mechighel F, Ismail T, Kolsi L, Ghachem K. Heat transfer and fluid flow in a PCM-filled enclosure: Effect of inclination angle and mid-separation fin. Int Commun Heat Mass Transf 2021;124:105280. [CrossRef]
[23] Pulagam MKR, Rout SK, Muduli KK, Syed SA, Barik D, Hussein AK. Internal finned heat exchangers: Thermal and hydraulic performance review. Int J Heat Technol 2024;42:583−592. [CrossRef]
[24] Pelella F, Zsembinszki G, Viscito L, Mauro AW, Cabeza LF. Thermo-economic optimization of a multi-source (air/sun/ground) residential heat pump with a water/PCM thermal storage. Appl Energy 2023;331:120398. [CrossRef]

[25] Voller VR, Prakash C. A fixed grid numerical modelling methodology for convection-diffusion mushy region phase-change problems. Int J Heat Mass Transf 1987;30:1709–1719. [CrossRef]

[26] Farid MM, Kanzawa A. Thermal performance of a heat storage module using PCM's with different melting temperatures: Mathematical modeling. J Sol Energy Eng 1989;111:152–157. [CrossRef]

[27] Patankar S. Numerical heat transfer and fluid flow. 1st ed. Boca Raton: CRC Press; 1980.

[28] Lacroix M. Numerical simulation of a shell-and-tube latent heat thermal energy storage unit. Sol Energy 1993;50:357–367. [CrossRef]

[29] Kenisarin M, Mahkamov K. Solar energy storage using phase change materials. Renew Sustain Energy Rev 2007;11:1913–1965. [CrossRef]

[30] Farid MM, Khudhair AM, Razack SAK, Al-Hallaj S. A review on phase change energy storage: Materials and applications. Energy Convers Manag 2004;45:1597–1615. [CrossRef]